CHEMISTRY
A EUROPEAN JOURNAL

ChemPubSoc
Europe

DOI: 10.1002/chem.201302662

Encapsulation and Release Mechanisms in Coordination Polymer Nanoparticles

Laura Amorín-Ferré,[a] Félix Busqué,[a] José Luis Bourdelande,[a] Daniel Ruiz-Molina,[b, c] Jordi Hernando,*[a] and Fernando Novio*[b, c]

Abstract: The interplay of guest encapsulation and release mechanisms in nanoscale metal–organic vehicles and its effect on the drug-delivery kinetics of these materials were investigated through a new multidisciplinary approach. Two rationally-designed molecular guests were synthesized, which consist of a red-fluorescent benzophenoxazine dye covalently tethered to a coordinating catechol group and a protected, non-coordinating catechol moiety. This allowed loading of the guests into compositionally and structurally equivalent coordination polymer particles through distinct encapsulation mechanisms: coordination and mechanical entrapment. The two types of particles delivered their fluorescent cargo with remarkably different kinetic profiles, which could be satisfactorily modeled considering degradation- and diffusion-controlled release processes. This demonstrates that careful selection of the method of guest incorporation into coordination polymer nanoparticles allows selective tuning of the rate of drug delivery from these materials and, therefore, of the time window of action of the encapsulated therapeutic agents.

Keywords: nanoparticles · drug delivery · fluorescence · metal–organic frameworks · polymers

Introduction

Coordination polymer particles (CPPs) have recently emerged as a new family of metal–organic materials formed by the self-assembly of metal ions and polydentate bridging ligands.[1,2] Together with crystalline metal–organic frameworks (MOFs), CPPs have been proposed for a large variety of applications owing to the intrinsic versatility of coordination chemistry, which allows the properties of the final materials to be rationally tailored by an appropriate choice of metals and ligands.[3] Of special interest is the use of CPPs in medicine, which is predicted to have a broad impact in the fields of bioimaging and drug delivery.[4–6] Since the pioneering work of Mirkin and co-workers in 2005,[1] an increasing number of reports have indeed described the successful application of nanoscale coordination polymer particles to encapsulate and release therapeutic agents.[6] Nonetheless, the use of CPPs for drug delivery is in its fledgling stage. A detailed rationalization of guest encapsulation and release mechanisms is still required to understand the drug-delivery kinetics of most CPPs and, consequently, to fully assess their potential use as nanocarriers for therapeutic purposes. Although these issues have already been subject of extensive debate for biodegradable organic polymer vehicles as drug-delivery systems,[7–9] little attention has so far been paid to them with regards to the emerging CPP-based materials.

Incorporation of the active molecules in coordination polymer nanoparticles usually proceeds through two distinct strategies: 1) binding of the drug to the polymer framework as a CPP building block[10–14] and 2) mechanical entrapment of the therapeutic agent within the metal–organic matrix.[15–17] Accordingly, drug release can take place though different mechanisms, namely slow particle degradation through surface erosion, fast diffusion processes and/or a combination of both. This scenario can be even more intricate if undesired desorption from the particle surface occurs. As a result, complex drug-delivery profiles are often encountered in CPPs that preclude unambiguous elucidation of the relationship between encapsulation and release mechanisms.[5,16]

To shed more light on this issue, we have envisioned the fabrication of morphologically equivalent CPPs bearing a fluorescent guest that can be either coordinated to the polymer backbone (**M1**) or physically encapsulated within the parti-

[a] L. Amorín-Ferré, Dr. F. Busqué, Dr. J. L. Bourdelande, Dr. J. Hernando
Departament de Química, Universitat Autònoma de Barcelona
Edifici C/n, Campus UAB, Cerdanyola del Vallès, 08193 (Spain)
Fax: (+34) 935811265
E-mail: jordi.hernando@uab.cat

[b] Dr. D. Ruiz-Molina, Dr. F. Novio
Institut Català de Nanociència i Nanotecnologia (ICN2)
Edifici ICN2, Campus UAB Cerdanyola del Vallès, 08193 (Spain)
Fax: (+34) 937372648
E-mail: fernando.novio@cin2.es

[c] Dr. D. Ruiz-Molina, Dr. F. Novio
Consejo Superior de Investigaciones Científicas (CSIC), Edificio ICN2, Campus UAB
Cerdanyola del Vallès, 08193(Spain)

Supporting information for this article is available on the WWW under http://dx.doi.org/10.1002/chem.201302662.

cle (**M2**). These two materials therefore represent excellent benchmark systems to comparatively investigate degradation- and diffusion-controlled drug-release processes in CPPs. A schematic representation of this approach is shown in Figure 1. The molecular guest of choice for these studies is a red-fluorescent benzophenoxazine dye covalently linked to a coordinating catechol group, both in its non-protected (**1**) and protected forms (**2**). On the other side, cobalt nanoparticles were used as carriers, with the general composition [Co(bix)(3,5-dbsq)(3,5-dbcat)], in which bix is a flexible bisimidazole bridging ligand and 3,5-dbsq and 3,5-dbcat represent the semiquinonate radical and catecholate forms of the 3,5-di-*tert*-butylcatechol, respectively.[15,16,18] Although analogous CPPs containing Zn^{II} ions and bix ligands have already been reported and evaluated for drug-delivery applications,[15,16] the choice of [Co(bix)(3,5-dbsq)(3,5-dbcat)] nanoparticles is justified by: 1) the high affinity of catechol groups to coordinate to cobalt ions, which provided us with a simple way to incorporate the fluorescent guest to the polymer backbone in **M1** without modification of the coordination sphere; 2) the well-known optical properties of [Co(3,5-dbsq)(3,5-dbcat)(N-N)] units,[19] which must result in efficient fluorescence quenching of compounds **1** and **2** while they remain in the interior of the nanoparticles and, therefore, allow for selective detection of the released guest molecules; and 3) the valence tautomerism exhibited by [Co(bix)(3,5-dbsq)(3,5-dbcat)] CPPs,[18] which can be exploited to assess the morphological similarities between **M1** and **M2**.

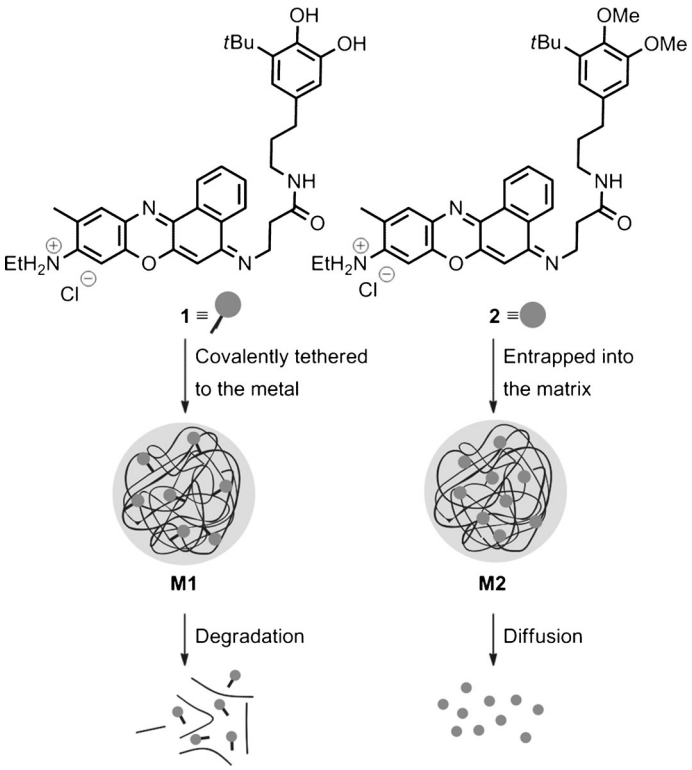

Figure 1. Chemical structures of fluorescent guest compounds **1** and **2**, with which **M1** and **M2** coordination polymer particles were prepared to investigate degradation- and diffusion-controlled release from CPPs.

Results and Discussion

Synthesis and characterization of fluorescent guests 1 and 2: Scheme 1 shows the synthetic route followed to obtain **1** and **2**. Briefly, the *tert*-butylation and subsequent allylic oxidation of commercial 2-methoxy-4-methylphenol gave the known aldehyde **3** in 97% yield,[20] which is a common intermediate for both target compounds. At this point, synthetic pathways diverged, either temporally protecting the hydroxyl groups of the catechol moiety as the corresponding methoxymethylethers (MOM), to obtain compound **1**, or permanently derivatizing them as the methyl ethers as found in compound **2**. Thus, known intermediate **4a** was obtained from **3** by sequential demethylation with BBr_3, and protection of the corresponding catechol with methoxymethylbro-

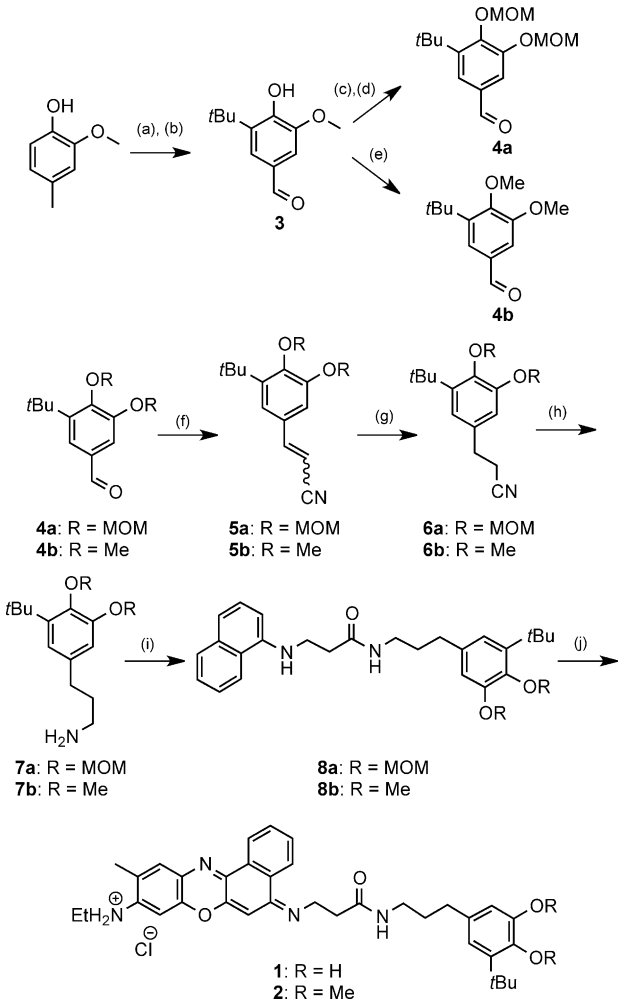

Scheme 1. Synthesis of fluorescent guests **1** and **2**. (a) *t*BuOH, H_3PO_4, 80°C, 10 h; (b) Br_2, *t*BuOH, RT, 4 h; (c) BBr_3, CH_2Cl_2, RT, 3 h; (d) MOM-Cl, *N*,*N*-diisopropylethylamine (DIPEA), 4-dimethylaminopyridine (DMAP), CH_2Cl_2, heat at reflux, 24 h; (e) Me_2SO_4, K_2CO_3, $(n\text{-}Bu)_4NI$, DMF, RT, 15 h; (f) Ph_3PCHCN, toluene, heat at reflux, 18 h; (g) H_2 (2 atm), Pd/C, EtOAc 18 h; (h) $LiAlH_4$, anhydrous THF, addition at 0°C, then RT, 15 h; (i) 3-(naphthalen-1-ylamino)propanoic acid, EDCI, DIPEA, CH_2Cl_2, RT, 18 h; (j) *N*-ethyl-5-hydroxy-2-methyl-4-nitrosobenzenaminium chloride, HCl, MeOH, heat at reflux, 2 h.

mide (90% overall yield).[21] Methylation of the free hydroxyl of compound **3** gave previously described derivative **4b** (90%).[22]

The next synthetic steps are analogous for both target compounds. The Wittig reaction between aldehydes **4a** and **4b** and the stabilized phosphorane 2-(triphenylphosphoranylidene)acetonitrile afforded the corresponding olefins **5a** (96% yield) and **5b** (72% yield), as mixtures of *Z*- and *E* isomers. Successive hydrogenation of the alkene moieties, at high pressure of H_2 under Pd/C catalyst, and nitriles, with $LiAlH_4$, furnished amines **7a** and **7b** in 61 and 51% overall yields for both reduction reactions, respectively. After this, troublesome formation of amides **8a** (31% yield) and **8b** (35% yield) was achieved by reaction between amines **7a** and **7b** and 3-(naphthalen-1-ylamino) propanoic acid, using 1-ethyl-3-(3-dimethyl aminopropyl)carbodiimide (EDCI) as a coupling agent.[23] Compounds **1** and **2** were finally obtained by reaction between naphthylamines **8a** and **8b** and *N*-ethyl-5-hydroxy-2-methyl-4-nitrosobenzenaminium chloride in methanol, under acidic catalyst and heated at reflux (45 and 35% yield for **1** and **2**, respectively).[24] Importantly, this last step did not only allow the benzophenoxazine dye group of both fluorescent guests to be constructed, but also concomitant cleavage of the methoxymethylethers to eventually obtain compound **1**.

Once synthesized, the optical properties of compounds **1** and **2** were investigated in detail. Figure 2 plots the absorption and fluorescence emission spectra of these species

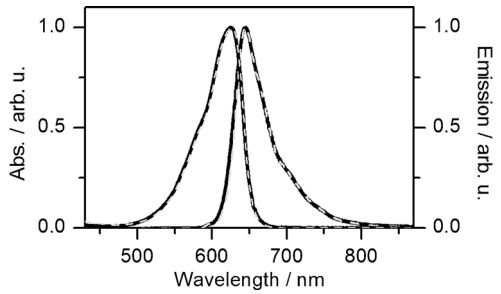

Figure 2. Absorption and fluorescence emission spectra of fluorescent guests **1** (——) and **2** (– – –).

in methanol, which are mainly governed by the optical transitions corresponding to their benzophenoxazine dye unit. As a result, compounds **1** and **2** display equivalent absorption ($\lambda_{max,1}=625$, $\lambda_{max,2}=626$ nm, $\varepsilon_{max,1}=\varepsilon_{max,2}=4.8\times10^4\,M^{-1}cm^{-1}$) and emission bands ($\lambda_{max,1}=643$, $\lambda_{max,2}=645$ nm), which resemble those reported for similar derivatives.[25] Importantly, covalent tethering of the benzophenoxazine unit to catechol and *o*-methoxyanisole groups in **1** and **2** does not quench its inherent emissive behavior, the resulting dyads thus presenting high fluorescence quantum yields ($\Phi_{f,1}=0.40$, $\Phi_{f,2}=0.41$). Together with their long-wavelength absorption and emission spectra, this makes compounds **1** and **2** ideal fluorescent reporters to monitor the guest release from CPPs as well as particle degradation.

Fabrication and characterization of M1 and M2 CPPs: Adapting an experimental procedure previously published by us,[18] coordination polymer particles **M1** and **M2** were prepared by reaction of Co^{II} ions with the ditopic ligands 1,4-bis(imidazol-1-ylmethyl)benzene and 3,5-di-*tert*-butylcatechol in the presence of guest compounds **1** and **2** (Figure 3a). This led to the formation of [Co(bix)(3,5-dbsq)(3,5-dbcat)] polymers, which readily precipitated as nanoparticles due to their low solubility in the reaction medium. The resulting CPPs were subsequently collected by centrifugation, washed with 5:1 water/ethanol mixtures until no red fluorescence was observed in the supernatant solution, and then dried. For comparison purposes, guest-free coordination polymer nanoparticles (**M0**) were also prepared using this methodology. Noticeably, very small amounts of compounds **1** and **2** were used in the preparation of materials **M1** and

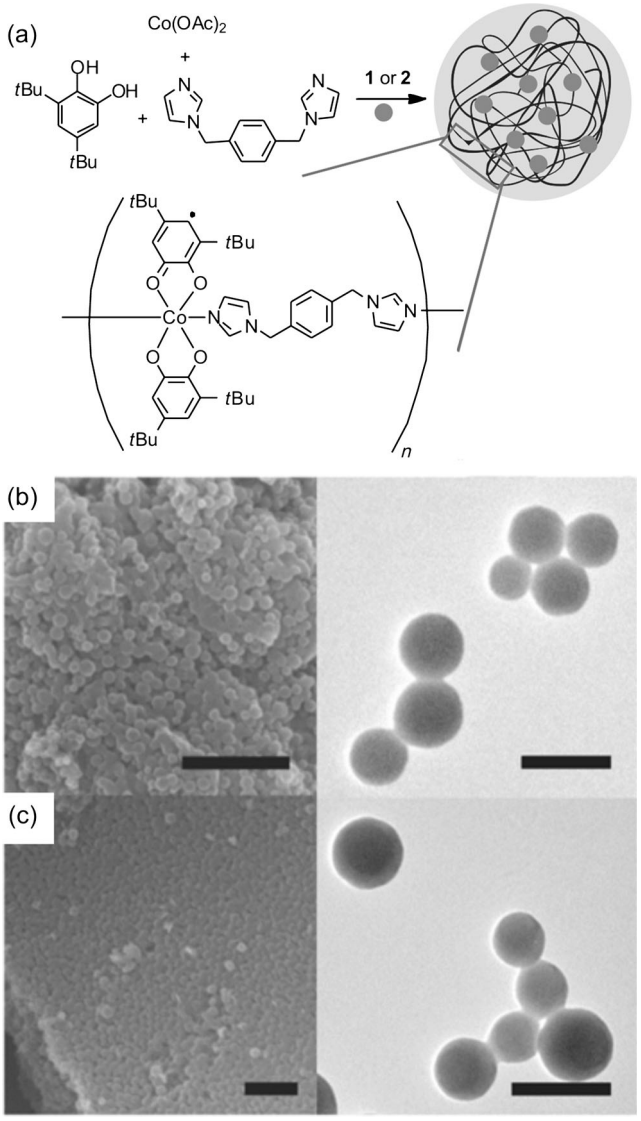

Figure 3. (a) Schematic synthesis of CPPs doped with fluorescent guests **1** and **2**; (b and c) SEM (left) and TEM (right) images of **M1** (b) and **M2** (c) particles. Scale bars for SEM are 1 μm and for TEM are 200 nm.

M2 (catechol/guest molar ratio ≈100:1). With such low doping loads we intended to minimize the effect of the fluorescent guests on the formation of the nanoparticles, which should allow us to unambiguously ascribe the differences observed in their release profiles to the occurrence of distinct guest incorporation and delivery mechanisms.

The formation of morphologically equivalent CPPs was indeed revealed by scanning (SEM) and transmission (TEM) electron microscopy images (Figure 3b and c, see also Figure S1 in the Supporting Information). In all cases, nanometer-sized solid particles with spherical shapes and rather uniform and similar diameters ((195±38), (152±22), and (185±37) nm for **M0**, **M1**, and **M2**, respectively) were obtained. X-ray diffraction experiments confirmed the amorphous character of these materials, whereas spectroscopic characterization upon dissolution of the nanoparticles in degassed methanol revealed the occurrence of different electronic absorption bands arising from their constituent functional units (Figure 4a). Thus, an absorption band at $\lambda \approx 625$ nm was selectively found in the spectra of **M1** and **M2**, which corresponds to the fluorescent benzophenoxazine moiety loaded in these materials. On the contrary, the other absorption bands at $\lambda \approx 400$, 590, and 700 nm were not only encountered in the spectra of **M1** and **M2**, but also observed for guest-free **M0**. These can be ascribed to intraligand and metal-to-ligand/ligand-to-metal charge-transfer electronic transitions of the [Co(bix)(3,5-dbsq)(3,5-dbcat)] system.[26] Noticeably, these absorption bands corresponding to the coordination complex units expand all over the UV/Vis and NIR regions, and therefore they overlap with the emission spectrum of the benzophenoxazine dye (see Figure 2a).

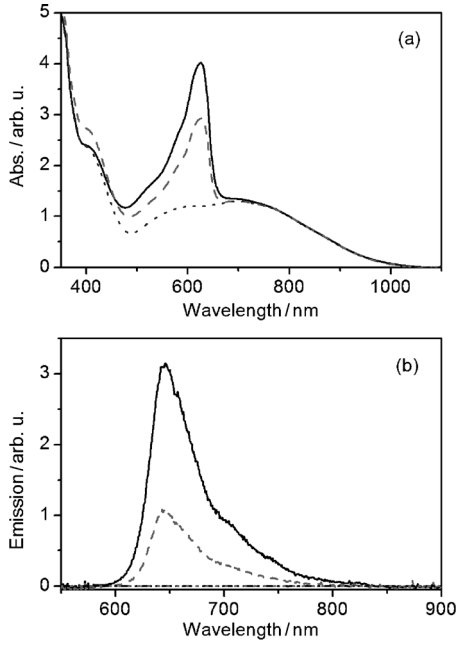

Figure 4. (a) Absorption spectra of **M0** (·····), **M1** (——), and **M2** (– – –) in degassed MeOH; (b) Fluorescence emission spectra recorded in degassed MeOH of **M1** (——) and **M2** (– – –) and in non-degassed MeOH of **M1** (–·–·) and **M2** (·····)

Consequently, efficient quenching of dye fluorescence through resonant energy-transfer processes is expected in the interior of the nanoparticles, where these moieties will be located at the near proximity of coordination complex units regardless of whether they are directly coordinated to the metal center or physically encapsulated within the polymer network. Indeed, no red fluorescence could be measured for **M1** and **M2** particles in the solid state and in degassed methanol, which confirms effective quenching of the emission of the loaded guests (Figure 4b).

Fluorescence quenching is however inhibited upon guest release and CPP degradation, which allowed us to monitor the delivery of the particle cargo by means of highly sensitive emission measurements (see below). This was demonstrated by measuring the optical properties of **M0**, **M1**, and **M2** in non-degassed methanol, in which particle dissolution is followed by coordination polymer degradation through ligand exchange and concomitant oxidation of the catecholate and semiquinone groups. This leads to the disappearance of the absorption bands associated to the [Co(bix)(3,5-dbsq)(3,5-dbcat)] coordination polymers as well as pronounced growth of the band at $\lambda \approx 400$ nm corresponding to the quinone species resulting from catecholate and semiquinone degradation (see Figure S2 in the Supporting Information).[27] Accordingly, no energy-transfer processes are expected under such conditions and an enormous increase in benzophenoxazine emission was indeed measured (Figure 4b). The absorption measurements in non-degassed methanol were also used to quantify the encapsulation efficiencies for the preparation of dye-doped **M1** and **M2** particles. Interestingly, higher values were obtained for **M1** (≈20%) than for **M2** (≈10%) under equivalent experimental conditions, which indicates that incorporation of the fluorescent guest bearing a coordinating catechol moiety is significantly more effective.

Valence tautomerism of M1 and M2 CPPs: The amorphous nature of **M1** and **M2** nanoparticles precludes any accurate structural characterization by classical diffraction techniques. Nevertheless, we exploited the valence tautomerism (VT) behavior shown by [Co(bix)(3,5-dbsq)(3,5-dbcat)] CPPs[18,19] to investigate the structural similarities between **M1** and **M2**. These systems might interconvert reversibly between the low-spin (*ls*)-[Co^{III}(bix)(3,5-dbsq)(3,5-dbcat)] and high-spin (*hs*)-[Co^{II}(bix)(3,5-dbsq)$_2$] tautomers by intramolecular metal–ligand electron-transfer, a process that can be selectively monitored by temperature-dependent measurements of magnetic susceptibility.

Figure 5 plots the results obtained in those measurements for **M0**, **M1**, and **M2**. In all cases, an abrupt change in effective magnetic moment (μ_{eff}) is observed around 300 K, which is consistent with valence-tautomeric interconversion from low- to high-spin states for a large fraction of molecules in the nanoparticles.[18] Importantly, the occurrence of valence tautomerism and the actual profile of the corresponding μ_{eff} versus T plot is not only highly sensitive to the composition and structure of the metal complex, but also to

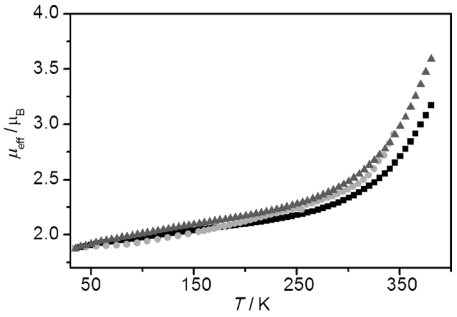

Figure 5. Values of μ_{eff} as a function of temperature for **M0** (▲), **M1** (■) and **M2** (●) CPPs.

the local environment.[19] In other words, the same complex may or may not exhibit VT, or the low-spin-to-high-spin conversion might take place at different temperatures depending on structural and environmental parameters. Therefore, the extremely similar magnetic behavior encountered for **M0**, **M1**, and **M2** clearly indicates that they must be formed by equivalent coordination polymers in rather comparable phases.

Guest release mechanisms: To investigate guest release from **M1** and **M2**, colloidal suspensions were prepared in phosphate-buffered saline solutions (PBS) at pH 7.4, placed in a dialysis bag (molecular weight cut-off (MWCO): 3500 Da) at 37 °C, and finally dialyzed against PBS for 100 h. Relative cumulative release profiles were then measured by monitoring the fluorescence of the dialysis bath solution in time. In addition, the solid material remaining in the dialysis bag after 100 h was dissolved in methanol and characterized by absorption spectroscopy, which allowed us to determine the absolute release efficiency of the dialysis experiment. Figure 6 plots the cumulative release profiles measured for **M1** and **M2** under these experimental conditions. Both exhibit very high release efficiencies after 100 h ($\approx$90 %) with no "burst effects" associated with undesired desorption of guest molecules physisorbed onto the nanoparticle surface. However, the release kinetics measured for these materials were found to be strikingly different. In the case of **M2**, the delivery process was nearly completed after 8 h ($t_{1/2}\approx$1.2 h), a behavior resembling that already reported for the release of anticancer drugs mechanically entrapped in analogous [Zn(bix)] CPPs.[16] In contrast, a much slower process was observed for **M1**, which required about 100 h for completion ($t_{1/2}\approx$11 h).

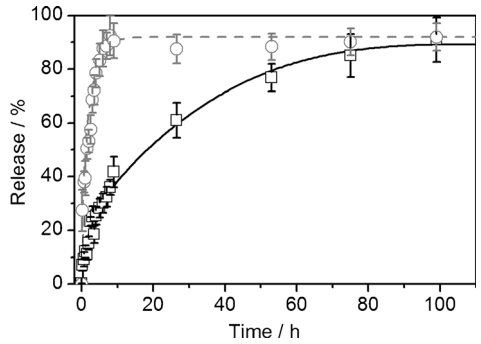

Figure 6. Guest release profiles of fluorescent guest molecules from **M1** (■) and **M2** (●) at 37 °C, which were averaged over 4 independent experiments. Lines correspond to fits of the experimental data as described in the text.

On the basis of the non-coordinating nature of the encapsulated guest, the release profile of **M2** at 37 °C was fitted with a purely diffusion-controlled model of drug delivery. In particular, we considered the use of Equation (1), which was derived for drug delivery through Fickian diffusion from spherical particles with homogenous and low-doping loads that do not significantly swell or degrade during the release process:[28]

$$M_t = M_\infty\left(1-\frac{6}{\pi^2}\sum_{n=1}^{\infty}\frac{1}{n^2}\exp\left(-\frac{Dn^2\pi^2 t}{R^2}\right)\right) \quad (1)$$

in which M_t and M_∞ represent the cumulative absolute amounts of guest released at time t and infinity, R is the radius of the particles and D is the apparent diffusion constant of the drug within the system. D is the only variable parameter in this model; however, it is taken to remain constant throughout the release process by neglecting swelling and degradation effects on the structure of the polymeric drug carrier.

As can be observed in Figure 6, a rather satisfactory fit of the experimental release kinetics of **M2** was obtained by using Equation (1). Therefore, the delivery of the mechanically entrapped fluorescent guest must be governed by a time-independent diffusion mechanism ($D=6.9\times10^{-19}\,m^2s^{-1}$), which indicates that the influence of degradation processes on the release kinetics is negligible in this case even though it takes place. This is proven by Figure 7, which displays SEM images of **M2** nanoparticles suspended in aqueous media at 37 °C for 0, 5, 26 and 100 h. While most particles preserved their spherical shape after 5 h, extensive surface erosion and an increasing amount of non-structured material is observed in the SEM images registered at 26 and 100 h. This confirms CPP degradation, which however takes place at a longer timescale than guest diffusion from the nanoparticles at 37 °C. This is in contrast with other systems for which clearly different delivery phases are observed that are ascribed to the occurrence of sequential fast diffusion and slow degradation processes.[7–9]

The release profile obtained for **M1** at 37 °C was also tentatively fitted with single-mechanism models, which in this case should solely account for degradation-controlled delivery. However, poor agreement between the experimental and fitted release profiles was obtained regardless of using surface-degradation-[29] or bulk-degradation[30] models of drug delivery. This suggests the occurrence of a more complex release process, which we attempted to model by assuming simultaneous delivery through degradation and diffusion processes. In this scenario, degradation-controlled release should apply for all guest molecules coordinated to the polymeric backbone, whereas those that remain unbound

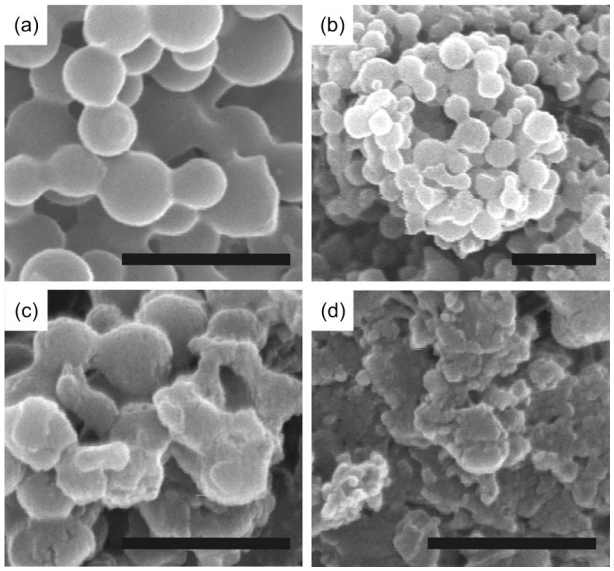

Figure 7. SEM images of **M2** CPPs suspended at 37 °C in aqueous media for (a) 0, (b) 5, (c) 26, and (d) 100 h. Scale bars are 500 nm.

but physically entrapped within the metal–organic matrix should be preferentially delivered by fast diffusion processes. Based on the previous results obtained for **M2** and analogous [Zn(bix)] CPPs,[16] Equation (2) was derived to account for such situation:

$$M_t = M_\infty\left(b\left(1-\frac{6}{\pi^2}\sum_{n=1}^{\infty}\frac{1}{n^2}\exp\left(-\frac{Dn^2\pi^2t}{R^2}\right)\right)+(1-b)\left(1-\left(1-\frac{k_dt}{(1-b)C_0R}\right)^3\right)\right) \quad (2)$$

The first term in this Equation corresponds to the Fickian diffusion model already applied to **M2**, in which b is the fraction of guest molecules that lie mechanically entrapped within **M1** particles. As previously discussed, this model assumes that the diffusion-controlled release of guest molecules takes place before significant degradation of the polymer matrix occurs, which allows the particle radius and the apparent guest diffusion constant to be considered time-independent. This assumption is not only supported by the behavior observed for **M2**, but also by the similar results obtained when monitoring the degradation process of **M1** nanoparticles at 37 °C in water media using SEM (see Figure S3 in the Supporting Information). The second term in Equation (2) corresponds to an empirical model that has been developed for degradation-controlled drug delivery from spherical particles through surface erosion,[29] which is indeed the degradation mechanism reported for analogous [Zn(bix)] CPPs at physiological conditions.[16] In this expression $(1-b)$ is the fraction of guest molecules coordinated to the metal centers in **M1**, k_d is the surface erosion rate constant, C_0 is the total initial concentration of the guest in the polymer matrix (7.2×10^{-4}% (w/w)) and R is the initial radius of the nanoparticles.

To fit Equation (2) to the guest release profile measured for **M1** at 37 °C, only two variable parameters were considered: b and k_d. To test the consistency of our model, D was directly taken from the previous fit of **M2** delivery kinetics, a rather plausible constraint based on the very similar structures of the guest compounds and coordination polymer particles investigated in this work. As observed in Figure 6, a good agreement was encountered between the experimental and fitted release profiles of **M1** even under such an assumption, which proves the validity of our treatment ($b=0.26$, $k_d/(C_0\times R)=1.7\times10^{-6}\,s^{-1}$). From this we conclude that most guest molecules in **M1** nanoparticles (74%) are directly bound to the polymer matrix, which are therefore released by slow degradation of the material. Nevertheless, a significant fraction of guest molecules (26%) are not coordinated to cobalt ions despite presenting free catechol groups, but they were physically encapsulated during the formation of the particles. Accordingly, they are delivered by a fast time-independent diffusion mechanism similar to that encountered for **M2** CPPs.

Additional guest release experiments were performed at 60 °C aimed at investigating the temperature dependence of the delivery processes in these materials (see Figure S4 in the Supporting Information). In deep contrast to what had been observed at 37 °C, no significant differences were found between the release profiles measured for **M1** and **M2** at this temperature. In both cases, complete delivery of the fluorescence guests is observed at ≈5 h, revealing the occurrence of much faster release processes. This suggests that the degradation kinetics accelerate enormously at 60 °C, which must become at least comparable to guest diffusion rates. As a matter of fact, we expect the release profiles of **M1** and **M2** CPPs at these conditions to be mainly governed by degradation processes, which indicate that both the guest delivery kinetics and mechanisms of these materials can be dramatically altered by temperature control.

Conclusion

In this work we report a new rational approach to investigate the relationship between guest encapsulation and release mechanisms for metal–organic nanoparticles. By appropriate design of the guest compounds and particle formation conditions, two types of coordination polymer particles were prepared that 1) are compositionally and structurally equivalent, and 2) were loaded with the same fluorescent guests using different encapsulation processes. As a result, the release of their fluorescent cargo at physiological conditions proceeds through distinct mechanisms that converge upon increasing the temperature. Physically encapsulated guest molecules are delivered by fast, time-independent diffusion processes, whereas the release of coordinated guest moieties is governed by slow particle degradation. This

leads to remarkably different guest delivery profiles for the CPPs prepared, which demonstrates that the kinetics of release can be selectively tuned up to many hours by appropriate choice of the mechanism of incorporation of the therapeutic agent into the polymeric nanocarrier. This result opens new venues for the future use of CPPs in medicine owing to the feasibility of loading drugs into these carriers by both mechanical entrapment and chemical binding to the metal centers. The former encapsulation mechanism has indeed already been demonstrated for anticancer drugs,[16] whereas tethering of these molecules to coordinating ligands could be attempted through functional groups that are readily cleaved at physiological conditions (e.g., ketals[31]), thus rendering the active form of the therapeutic agent after degradation-induced release from the polymer particles. As a result, controlling the ratio of coordinated versus physically entrapped drug molecules within CPPs would eventually allow tailoring the release kinetics to meet the therapeutic needs.

Experimental Section

Materials and characterization: All reactants and reagents were purchased from Sigma–Aldrich and used as received. Solvents were purchased from Scharlab and used as received. Dialysis bags were purchased from Orange Scientific. Infrared spectra were recorded on a Bruker Tensor 27 spectrometer equipped with a Golden Gate Single Reflection Diamond attenuated total reflectance (ATR) accessory. High-resolution mass analyses were performed on an ESI-QTOF Bruker Daltonics micrOTOF-Q spectrometer. NMR spectra were recorded on a Bruker ARX 400 (400 MHz for ^{1}H NMR and 100 MHz for ^{13}C NMR). The spectra are given in δ (ppm) using the signal of the residual non-deuterated solvent molecules as reference. Absorption spectra were recorded on a Hewlett Packard 8453 spectrophotometer. HPLC or spectroscopy quality solvents were used. Emission spectra were measured by means of a custom-made spectrofluorimeter, in which a continuous wave (CW) He–Ne Research Electro Optics (REO) laser ($\lambda_{exc}=594$ nm) was used as excitation source and the emitted photons were detected in an Andor ICCD camera coupled to a spectrograph. HPLC or spectroscopy quality solvents were used. Fluorescence quantum yields were determined using Nile Blue A in ethanol solution as reference ($\Phi_f=0.27$).[32] SEM measurements were registered on a HITACHI S-570 microscope (accelerating voltage 0.5–30 kV). TEM measurements were carried out on a HITACHI-7000 microscope operating at 125 kV.

Synthesis of 4a: This compound was prepared according to ref. [21] with some modifications.

Demethylation: A solution of BBr_3 (4 mL of 1 M) in CH_2Cl_2 was added drop-wise into a solution of **3** (0.845 g, 4 mmol) in CH_2Cl_2 (30 mL) cooled down in a liquid nitrogen bath. The reaction was allowed to proceed at room temperature for 2 h. The reaction mixture was then poured into distilled water (40 mL) and the resulting aqueous layer was extracted twice with CH_2Cl_2 (30 mL). The organic extracts were dried with $MgSO_4$ and the solvent evaporated under vacuum to afford the demethylated compound as a yellowish solid (0.698 g, 90%). This compound was used in the next step without further purification.

Protection of the catechol: DIPEA (2.7 mL, 15.5 mmol), DMAP (30 mg, 0.22 mmol), and methoxymethyl bromide (0.65 mL, 8.02 mmol) were added drop-wise into a solution of the above intermediate (0.492 g, 2.54 mmol) in CH_2Cl_2 (8 mL) cooled down in a water bath. The solution was heated at reflux for 8 h. The reaction mixture was treated with water (15 mL) and the resulting aqueous layer was extracted twice with CH_2Cl_2 (15 mL). The organic extracts were dried with $MgSO_4$ and the solvent evaporated under vacuum. The crude product was purified by flash chromatography using hexanes and ethyl acetate (4:1, v/v) to afford **4a** (0.716 g, 100%) as a yellowish oil. ^{1}H NMR (400 MHz, $CDCl_3$, 25 °C, TMS): $\delta=9.87$ (s, 1H), 7.55 (s, 2H), 5.31 (s, 2H), 5.23 (s, 2H), 3.66 (s, 3H), 3.52 (s, 3H), 1.45 ppm (s, 9H); ^{13}C NMR (100 MHz, $CDCl_3$, 25 °C, TMS): $\delta=191.5$, 151.9, 150.4, 144.0, 131.5, 123.8, 114.5, 99.4, 95.4, 57.9, 56.6, 35.4, 30.3 ppm; IR (ATR): $\tilde{\nu}=3076.2$, 2953.3, 2905.4, 2826.8, 1690.1, 1578.5 cm^{-1}; HRMS (ESI-QTOF): *m/z* calcd for $C_{15}H_{22}NaO_5$: 305.1359; found: 305.1356.

Synthesis of 4b: This compound was prepared according to ref. [22] with some modifications. K_2CO_3 (6.95 g, 50.4 mmol) and *N,N,N*-tributyl-1-butanaminium iodide (270 mg, 0.73 mmol) were added to a solution of **3** (3.5 g, 16.8 mmol) in DMF (100 mL),. The reaction mixture was stirred for 2 h at room temperature. After this time, Me_2SO_4 (3.2 mL, 33.6 mmol) was added drop-wise and the mixture was allowed to react for 16 h. The resulting mixture was treated with water (100 mL) and the aqueous layer was extracted four times with EtOAc (50 mL). The organic extracts were dried with $MgSO_4$ and the solvent evaporated under vacuum to afford **4b** (3.36 g, 90%) as a dark-green oil. ^{1}H NMR (400 MHz, $CDCl_3$, 25 °C, TMS): $\delta=9.91$ (s, 1H), 7.48 (d, $J=1.9$ Hz, 1H), 7.38 (d, $J=1.9$ Hz, 1H), 3.97 (s, 3H), 3.94 (s, 3H), 1.44 ppm (s, 9H).

Synthesis of 5a: (Triphenylphosphoranylidene)acetonitrile (2.070 g, 6.87 mmol) was added to a solution of **4a** (1.559 g, 5.53 mmol) in toluene (45 mL). The reaction mixture was heated at reflux for 12 h, after which the solvent was evaporated under vacuum and the residue was purified by flash chromatography using hexanes and ethyl acetate (6:1, v/v) to afford a mixture of (*E*)- and (*Z*)-**5a** (1.621 g, 96%) as a brown oil with a diastereomeric ratio of 2.3:1. ^{1}H NMR (400 MHz, $CDCl_3$, 25 °C, TMS): $\delta=7.57$ (d, $J=2.2$ Hz, 1H), 7.47 (d, $J=2.2$ Hz, 1H), 7.32 (d, $J=16.6$ Hz, 1H), 7.16 (d, $J=2.2$ Hz, 1H), 7.06 (d, $J=2.2$ Hz, 1H), 7.03 (d, $J=12.0$ Hz, 1H), 5.75 (d, $J=16.6$ Hz, 1H), 5.34 (d, $J=12.0$ Hz, 1H), 5.26 (s, 2H), 5.24 (s, 2H), 5.21 (s, 2H), 5.19 (s, 2H), 3.66 (s, 3H), 3.65 (s, 3H), 3.53 (s, 3H), 3.51 (s, 3H), 1.43 (s, 9H), 1.41 ppm (s, 9H); ^{13}C NMR (100 MHz, $CDCl_3$, 25 °C, TMS): $\delta=150.7$, 150.5, 150.0 148.9, 148.7, 148.6, 143.9, 143.8, 128.6, 128.5, 122.5, 121.0, 118.6, 117.9, 115.0, 112.5, 99.3, 99.3, 95.5, 95.4, 94.8, 93.4, 57.9, 57.9, 56.5, 56.6, 35.5, 35.3, 30.4, 30.3 ppm; IR (ATR): $\tilde{\nu}=3371.2$, 2953.8, 2213.6, 1615.5, 1428.9 cm^{-1}; HRMS (ESI-QTOF): *m/z* calcd for $C_{15}H_{22}NaO_5$: 328.1519; found: 328.1519.

Synthesis of 5b: Synthesized from **4b** using the same procedure as for **5a**. Yield = 72% with a diastereomeric *E*/*Z* ratio of 4.8:1. ^{1}H NMR (400 MHz, $CDCl_3$, 25 °C, TMS): $\delta=7.53$ (d, $J=2.1$ Hz, 1H), 7.34 (d, $J=16.5$ Hz, 1H), 7.23 (d, $J=2.1$ Hz, 1H), 7.05 (d, $J=12.1$ Hz, 1H), 7.00 (d, $J=2.0$ Hz, 1H), 6.88 (d, $J=2.0$ Hz, 1H), 5.75 (d, $J=16.5$ Hz, 1H, 4.39 (d, $J=12.1$ Hz, 1H), 3.92 (s, 3H), 3.92 (s, 3H), 3.90 (s, 3H), 3.88 (s, 3H), 1.39 (s, 9H), 1.37 ppm (s, 9H); ^{13}C NMR (100 MHz, $CDCl_3$, 25 °C, TMS): $\delta=153.7$, 153.4, 151.7, 151.2, 151.0, 149.2, 144.1, 143.7, 128.5, 128.4, 122.0, 119.9, 119.8, 118.6, 110.2, 108.6, 94.5, 92.9, 60.7, 60.7, 56.0, 56.0, 35.3, 35.3, 30.4, 30.4 ppm; IR (ATR): $\tilde{\nu}=2952.0$, 2213.3, 1615.6, 1571.5, 1415.0, 1142.9, 1067.0, 1023.7 cm^{-1}; HRMS (ESI-QTOF): *m/z* calcd for $C_{15}H_{19}NaNO_2$: 268.1308, found: 268.1309.

Synthesis of 6a: A mixture of (*E*)- and (*Z*)-**5a** (1.442 g, 4.8 mmol) and 10% Pd/C (5:1, substrate/catalyst) in ethyl acetate (16 mL) was stirred at room temperature under a hydrogen atmosphere for 24 h. Next, Pd/C was filtered off and the solvent was removed in vacuo. The residue was purified by flash chromatography using hexanes and ethyl acetate (3:1, v/v) to afford **6a** (1.003 g, 68%) as a brown oil. ^{1}H NMR (400 MHz, $CDCl_3$, 25 °C, TMS): $\delta=6.90$ (d, $J=2.1$ Hz, 1H), 6.84 (d, $J=2.1$ Hz, 1H), 5.18 (s, 2H), 5.16 (s, 2H), 3.64 (s, 3H), 3.51 (s, 3H), 2.88 (t, $J=7.4$ Hz, 2H), 2.58 (t, $J=7.4$ Hz, 2H), 1.41 ppm (s, 9H); ^{13}C NMR (100 MHz, $CDCl_3$, 25 °C, TMS): $\delta=150.6$, 145.0, 143.9, 133.0, 120.6, 119.2, 114.7, 99.1, 95.6, 57.6, 56.4, 35.3, 31.7, 30.6, 19.6 ppm; IR (ATR): $\tilde{\nu}=2952.2$, 2904.6, 2826.2, 2374.0, 1602.7, 1433.6, 1154.6, 936.8 cm^{-1}; HRMS (ESI-QTOF): *m/z* calcd for $C_{17}H_{25}NaNO_4$: 330.1376; found: 330.1375.

Synthesis of 6b: Synthesized from **5b** using the same procedure as for **6a**. Yield = 67%. ^{1}H NMR (400 MHz, $CDCl_3$, 25 °C, TMS): $\delta=6.74$ (d, $J=2.1$ Hz, 1H), 6.69 (d, $J=2.1$ Hz, 1H), 3.86 (s, 6H), 2.90 (t, $J=7.4$ Hz, 2H), 2.60 (t, $J=7.4$ Hz, 2H), 1.37 ppm (s, 9H); ^{13}C NMR (100 MHz, $CDCl_3$, 25 °C, TMS): $\delta=171.5$, 153.7, 148.0, 144.0, 133.0, 119.7, 119.0,

111.0, 60.8, 56.0, 35.0, 32.2, 30.9 ppm; IR (ATR): $\tilde{\nu}$ = 2951.4, 2866.4, 2831.8, 2245.0, 1688.2, 1580.1, 1421.9, 1346.7, 1260.0, 1067.6, 1006.1 cm^{-1}; HRMS (ESI-QTOF): *m/z* calcd for $C_{15}H_{21}NaNO_2$: 270.1465; found: 270.1465.

Synthesis of 7a: A solution of **6a** (695 mg, 2.2 mmol) in anhydrous Et_2O (2 mL) was added drop-wise to a suspension of $LiAlH_4$ (298 mg, 7.9 mmol) in anhydrous Et_2O (2 mL) cooled down in a water bath. The reaction mixture was then stirred at room temperature for 14 h under an inert atmosphere. Next, the reaction mixture was cooled down to 0 °C and quenched with NaOH 1 M (15 mL). The resulting aqueous layer was extracted with Et_2O (15 mL) and $CHCl_3$ (15 mL). The combined organic extracts were dried with $MgSO_4$ and the solvent removed in vacuo to afford **7a** (627 mg, 89 %) as a yellowish oil. This product was used without further purification. ^{1}H NMR (400 MHz, $CDCl_3$ 25 °C, TMS): δ = 6.85 (d, *J* = 2.0 Hz, 1H), 6.80 (d, *J* = 2.0 Hz, 1H), 5.17 (s, 2H), 5.16 (s, 2H), 3.64 (s, 3H), 3.50 (s, 3H), 2.73 (t, *J* = 7.6 Hz, 2H), 2.58 (t, *J* = 7.6 Hz, 2H), 1.74 (q_t, *J* = 7.6 Hz, 2H), 1.40 ppm (s, 9H); ^{13}C NMR (100 MHz, $CDCl_3$, 25 °C, TMS): δ = 150.2, 143.9, 143.3, 137.2, 120.6, 114.7, 99.1, 95.5, 57.6, 56.4, 42.1, 35.7, 35.2, 33.4, 30.7 ppm; IR (ATR): $\tilde{\nu}$ = 3362.8, 2949.4, 1578.6, 1431.9, 1076.7, 961.7 cm^{-1}; HRMS (ESI-QTOF): *m/z* calcd for $C_{17}H_{29}NNaO_4$: 334.1989; found: 334.1979.

Synthesis of 7b: Synthesized from **6b** using the same procedure as for **7a**. Yield = 76 %. ^{1}H NMR (400 MHz, [D_4]MeOD, 25 °C, TMS): δ = 6.74 (d, *J* = 2.0 Hz, 2H), 3.82 (s, 3H), 3.80 (s, 3H), 2.70 (t, *J* = 7.5 Hz, 2H), 2.58 (t, *J* = 7.5 Hz, 2H), 1.79 (q_t, *J* = 7.5 Hz, 2H), 1.34 ppm (s, 9H); ^{13}C NMR (100 MHz, [D_4]MeOD, 25 °C, TMS): δ = 153.5, 146.9, 142.7, 136.8, 118.7, 111.3, 59.8, 55.3, 40.8, 34.8, 33.9, 33.3, 30.2 ppm; IR (ATR): $\tilde{\nu}$ = 3452.3, 2936.2, 1578.1, 1421.9, 1321.1, 1262.1, 1144.8, 1066.5, 1008.1 cm^{-1}; HRMS (ESI-QTOF): *m/z* calcd for $C_{15}H_{25}NNaO_2$: 252.1958; found: 252.1963.

Synthesis of 8a: A solution of **7a** (956 mg, 3 mmol) in anhydrous CH_2Cl_2 (10 mL) was added to a solution of 3-(naphthalen-1-ylamino)propanoic acid (646 mg, 3 mmol), 1-hydroxybenzotriazole (HOBt; 589 mg, 4.3 mmol), EDCI (760 mg, 3.9 mmol) and DIPEA (1.6 mL, 9.1 mmol) in 20 mL of anhydrous CH_2Cl_2,. The reaction mixture was stirred at room temperature for 17 h. Then, it was washed twice with a solution of saturated $NaHCO_3$ (10 mL) and once with a solution of saturated NaCl (10 mL). The organic layer was dried with $MgSO_4$ and solvent was evaporated under vacuum. The crude product was purified by flash chromatography using hexanes and ethyl acetate (1:1, v/v) to afford **8a** (482 mg, 31 %) as a brown oil. ^{1}H NMR (400 MHz, $CDCl_3$, 25 °C, TMS): δ = 7.81 (d, *J* = 8.1 Hz, 1H), 7.74 (d, *J* = 7.6 Hz, 1H), 7.38–7.23 (m, 4H), 6.79 (d, *J* = 1.9 Hz, 1H), 6.4 (d, *J* = 1.9 Hz, 1H), 6.58 (d, *J* = 7.6 Hz, 1H), 6.04 (s, 1H), 5.16 (s, 2H), 5.11 (s, 2H), 3.63 (s, 3H), 3.54 (t, *J* = 6.02 Hz, 2H), 3.46 (s, 3H), 3.24 (dd, *J* = 13.1 Hz, *J* = 6.7 Hz, 2H), 2.50 (m, 4H), 1.73 (q_t, *J* = 7.6 Hz, 2H), 1.39 ppm (s, 9H); ^{13}C NMR (100 MHz, $CDCl_3$, 25 °C, TMS): δ = 171.9, 150.1, 143.4, 143.1, 136.23, 134.4, 128.6, 126.5, 125.9, 124.9, 123.9, 120.4, 117.8, 114.5, 104.5, 99.0, 95.4, 57.6, 56.4, 40.4, 39.3, 35.3, 35.2, 33.3, 31.2, 30.7 ppm; IR (ATR): $\tilde{\nu}$ = 3304.4, 2949.4, 1638.2, 1580.4, 1526.7, 1199.4, 1035.5, 961.9 cm^{-1}; HRMS (ESI-QTOF): *m/z* calcd for $C_{30}H_{40}N_2NaO_5$: 531.2829; found: 531.2834.

Synthesis of 8b: Synthesized from **7b** by using the same procedure as for **8a**. Yield = 35 %. ^{1}H NMR (400 MHz, [D_4]MeOD, 25 °C, TMS): δ = 7.93 (d, *J* = 8.1 Hz, 1H), 7.69 (d, *J* = 7.9 Hz, 1H), 7.41–7.23 (m, 3H), 7.14 (d, *J* = 8.1 Hz, 1H), 6.69 (d, *J* = 2.9 Hz, 1H), 6.69 (s, *J* = 2.9 Hz, 1H), 6.65 (s, 1H), 6.60 (d, *J* = 4.3 Hz, 2H), 3.76 (s, 3H), 3.69 (s, 3H), 3.54 (t, *J* = 6.60 Hz, 2H), 3.17 (t, *J* = 7.00 Hz, 3H), 2.59 (t, *J* = 6.60 Hz, 2H), 2.53–2.45 (m, 4H), 1.73 (q_t, *J* = 7.6 Hz, 2H), 1.31 ppm (s, 9H); ^{13}C NMR (101 MHz, [D_4]MeOD, 25 °C, TMS): δ = 174.6, 154.3, 147.7, 144.7, 143.5, 137.6, 135.8, 129.3, 127.6, 126.6, 125.4, 125.1, 121.7, 119.5, 118.1, 112.1, 105.1, 60.7, 56.1, 41.6, 40.0, 36.3, 35.8, 34.2, 32.3, 31.1 ppm; IR (ATR): $\tilde{\nu}$ = 2919.5, 2478.6, 2065.58, 1627.1, 1577.7, 1450.4, 1420.8, 1143.8, 1067.9 cm^{-1}; HRMS (ESI-QTOF): *m/z* calcd for $C_{28}H_{36}N_2NaO_3$: 449.2799; found: 449.2804.

Synthesis of 1: To a solution of *N*-ethyl-5-hydroxy-2-methyl-4-nitrosobenzenaminium chloride (72 mg, 0.4 mmol) in MeOH (1 mL) cooled down in a water bath and under an inert atmosphere, a solution of **8a** (170 mg, 0.33 mmol) in degassed MeOH (1 mL) and a 3 droplets of HCl 35 % were added. This mixture was heated at reflux for 1.5 h. Then, it was cooled to room temperature and CH_2Cl_2 (5 mL) and a mixture of saturated NaCl (2 mL) and 3 droplets of HCl 35 % were added. The resulting organic layer was washed twice with saturated $NaHCO_3$ (3 mL) and once with saturated NaCl (3 mL). Next, it was dried with $MgSO_4$ and the solvent was removed in vacuo. Crude was purified by flash chromatography using CH_2Cl_2 and MeOH (10:1, v/v) to afford **1** (87 mg, 45 %) as a bluish-violet solid. ^{1}H NMR (400 MHz, [D_4]MeOD, 25 °C, TMS): δ = 8.73 (d, *J* = 8.1 Hz, 1H), 8.22 (d, *J* = 8.1 Hz, 1H), 7.82 (t, *J* = 7.5 Hz, 1H), 7.71 (t, *J* = 7.5 Hz, 1H), 7.51 (s, 1H), 6.90 (s, 1H), 6.70 (s, 1H), 6.40 (s, 1H), 6.38 (s, 1H), 3.95 (t, *J* = 6.2 Hz, 2H), 3.49 (q, *J* = 7.2 Hz, 3H), 3.21 (m, 2H), 2.75 (t, *J* = 6.2 Hz, 2H), 2.35 (m, 2H), 2.29 (s, 3H), 1.67 (q_t, *J* = 7.2 Hz, 2H), 1.46 ppm (s, 9H); ^{13}C NMR (100 MHz, [D_4]MeOD, 25 °C, TMS): δ = 172.9 158.2, 156.9, 152.5, 149.3, 145.7, 143.3, 136.8, 133.9, 132.9, 132.6, 132.5, 132.4, 132.3, 130.7, 129.0, 125.5, 124.5, 123.6, 118.2, 113.5, 94.5, 94.1, 41.9, 40.3, 39.8, 35.8, 34.0, 32.5, 30.1, 17.8, 14.2 ppm; IR (ATR): $\tilde{\nu}$ = 3213.7, 3076.2, 2921.8, 2852.5, 1640.1, 1587.6, 1540.9, 1433.8, 1307.7, 1160.8 cm^{-1}; HRMS (ESI-QTOF): *m/z* calcd for $C_{35}H_{41}N_4O_4^+$: 581.3122; found: 581.3124.

Synthesis of 2: Synthesized from **8b** using the same procedure as for **1**. Yield = 35 %. ^{1}H NMR (250 MHz, [D_4]MeOD, 25 °C, TMS): δ = 8.70 (d, *J* = 8.1 Hz, 1H), 8.20 (d, *J* = 8.1 Hz, 1H), 7.81 (t, *J* = 7.6 Hz, 1H), 7.70 (t, *J* = 7.6 Hz, 1H), 7.48 (s, 1H), 6.91 (s, 1H), 6.70 (s, 1H), 6.51 (s, 1H), 6.49 (s, 1H), 4.56 (s, 2H), 3.97 (t, *J* = 5.9 Hz, 2H), 3.74 (s, 3H), 3.70 (s, 3H), 3.49 (q, *J* = 6.2 Hz, 2H), 3.22 (t, 2H, *J* = 6.8 Hz, 2H), 2.77 (t, *J* = 5.9 Hz, 2H), 2.39 (t, *J* = 6.8 Hz, 2H), 2.28 (s, 3H), 1.68 (q_t, *J* = 6.8 Hz, 2H), 1.43–1.23 ppm (m, 12H); ^{13}C NMR (63 MHz, [D_4]MeOD, 25 °C, TMS): δ = 173.0, 158.2, 156.8, 154.3, 152.5, 149.2, 147.8, 143.6, 140.2, 137.4, 133.9, 132.9, 132.6, 132.2, 130.7, 129.0, 125.5, 124.5, 123.6, 119.4, 114.7, 112.1, 94.5, 60.7, 56.2, 41.9, 40.2, 39.8, 35.7, 34.9, 34.2, 33.0, 32.4, 31.9, 31.1 ppm; IR (ATR): $\tilde{\nu}$ = 2920.8, 2851.6, 1640.4, 1588.1, 1541.4, 1451.0, 1310.0, 1160.9, 1133.6, 1006.6 cm^{-1}; HRMS (ESI-QTOF): *m/z* calcd for $C_{37}H_{44}N_4NaO_4$: 609.3435; found: 609.3435.

Synthesis of M0: To a solution of di-*tert*-butylcathecol (107.2 mg, 0.48 mmol) and 1,4-bis(imidazol-1-ylmethyl)benzene (59.6 mg, 0.25 mmol) in EtOH (5 mL), an aqueous solution of [Co($CH_3COO)_2$]·$4H_2O$ (1 mL, 61.7 mg, 0.24 mmol) was added drop-wise. The mixture was stirred for 10 min and then the formation of nanoparticles was induced by fast addition of miliQ H_2O (25 mL). The excess ligand was removed by centrifugation and the nanoparticles were washed three times with H_2O.

Synthesis of M1: An aqueous solution (4 mL) of [Co($CH_3COO)_2$]·$4H_2O$ (121.4 mg, 0.49 mmol) were added drop-wise to a solution of **1** (5.5 mg, 9.5 μmol), di-*tert*-butylcathecol (211.5 mg, 0.95 mmol) and 1,4-bis(imidazol-1-ylmethyl)benzene (117.3 mg, 0.49 mmol) in EtOH (20 mL). The mixture was stirred for 10 min and then the formation of nanoparticles was induced by fast addition of miliQ H_2O (100 mL). Ligand excess was removed by centrifugation and the nanoparticles were washed with a mixture of EtOH/H_2O (v/v 1:5) until no red fluorescence was observed from the supernatant solution.

Synthesis of M2: An aqueous solution (2 mL) of [Co($CH_3COO)_2$]·$4H_2O$ (68.9 mg, 0.28 mmol) was added drop-wise to a solution of **2** (3.1 mg, 5.1 μmol), di-*tert*-butylcathecol (120 mg, 0.53 mmol) and 1,4-bis(imidazol-1-ylmethyl)benzene (65 mg, 0.27 mmol) in EtOH (10 mL). The mixture was stirred for 10 min and then the formation of the nanoparticles was induced by fast addition of miliQ H_2O (50 mL). The excess ligand was removed by centrifugation and the nanoparticles were washed with a mixture of EtOH/H_2O (v/v 1:5) until no red fluorescence was observed from the supernatant solution.

Guest release experiments: A dialysis bag (MWCO: 3500) containing **M1** or **M2** (ca. ≈3 mg mL^{-1}) dispersed in phosphate buffered saline solution (PBS; pH 7.4) was placed into a solution of PBS (150 mL, pH 7.4; dialysate) at 37 °C under light stirring. To determine the increase in the concentration of **1** or **2** diffused through the dialysis bag, aliquots of the external PBS solution (0.5 mL) were taken from the dialysate at prefixed times and diluted in MeOH (2 mL), and each aliquot was analyzed by fluorescence spectroscopy. The solid material remaining in the dialysis

bag after 100 h was dissolved in methanol and characterized by using absorption spectroscopy.

Acknowledgements

We acknowledge the financial support of the "Ministerio de Economía y Competividad" (MINECO) through projects MAT2012–38318-C03–02, MAT2012–38319-C02–01, CTQ2012–30853 and CTQ2010–15380. L.A.-F. thanks the "Universitat Autònoma de Barcelona" for a pre-doctoral grant. F.N. thanks the "Ministerio de Economía y Competitividad" for a JdC (JCI-2011–09239) post-doctoral grant.

[1] M. Oh, C. A. Mirkin, *Nature* **2005**, *438*, 651–654.
[2] X. Sun, S. Dong, E. Wang, *J. Am. Chem. Soc.* **2005**, *127*, 13102–131103.
[3] A. M. Spokoyny, D. Kim, A. Sumrein, C. A. Mirkin, *Chem. Soc. Rev.* **2009**, *38*, 1218–1227.
[4] J. Della Rocca, D. Liu, W. Lin, *Acc. Chem. Res.* **2011**, *44*, 957–968.
[5] Z. Ma, B. Moulton, *Coord. Chem. Rev.* **2011**, *255*, 1623–1648.
[6] F. Novio, J. Simmchen, N.-A. Vázquez, L. Amorín, D. Ruiz-Molina, *Coord. Chem. Rev.* **2013**, *257*, 2839.
[7] J. Siepmann, A. Göpferich, *Adv. Drug Delivery Rev.* **2001**, *48*, 229–247.
[8] D. Y. Arifin, L. Y. Lee, C.-H. Wang, *Adv. Drug Delivery Rev.* **2006**, *58*, 1274–1325.
[9] L. L. Lao, N. A. Peppas, F. Y. C. Boey, S. S. Venkatraman, *Int. J. Pharm.* **2011**, *418*, 28–41.
[10] W. J. Rieter, K. M. Pott, K. M. L. Taylor, W. Lin, *J. Am. Chem. Soc.* **2008**, *130*, 11584–11585.
[11] J. Yang, W. Liu, M. Sui, J. Tang, Y. Shen, *Biomaterials* **2011**, *32*, 9136–9143.
[12] L. Xing, Y. Cao, S. Che, *Chem. Commun.* **2012**, *48*, 5995–5997.
[13] R. C. Huxford, K. E. de Krafft, W. S. Boyle, D. Liu, W. Lin, *Chem. Sci.* **2012**, *3*, 198–204.
[14] K. Wang, X. Ma, D. Shao, Z. Geng, Z. Zhang, Z. Wang, *Cryst. Growth Des.* **2012**, *12*, 3786–3791.
[15] I. Imaz, J. Hernando, D. Ruiz-Molina, D. Maspoch, *Angew. Chem.* **2009**, *121*, 2361–2365; *Angew. Chem. Int. Ed.* **2009**, *48*, 2325–2329.
[16] I. Imaz, M. Rubio-Martínez, L. García-Fernández, F. García, D. Ruiz-Molina, J. Hernando, V. Puntes, D. Maspoch, *Chem. Commun.* **2010**, *46*, 4737–4739.
[17] P. Huang, J. Mao, L. Yang, P. Yu, L. Mao, *Chem. Eur. J.* **2011**, *17*, 11390–11393.
[18] I. Imaz, D. Maspoch, C. Rodríguez-Blanco, J. M. Pérez-Falcón, J. Campo, D. Ruiz-Molina, *Angew. Chem.* **2008**, *120*, 1883–1886; *Angew. Chem. Int. Ed.* **2008**, *47*, 1857–1860.
[19] a) E. Evangelio, D. Ruiz-Molina, *Eur. J. Inorg. Chem.* **2005**, 2957–2971; b) D. N. Hendrickson, C. G. Pierpont, *Top. Curr. Chem.* **2004**, *234*, 63–95; c) P. Gütlich, A. Dei, *Angew. Chem.* **1997**, *109*, 2852–2855; *Angew. Chem. Int. Ed. Engl.* **1997**, *36*, 2734–2736.
[20] Q. Wang, Y. Yang, Y. Li, W. Yu, Z. J. Hou, *Tetrahedron* **2006**, *62*, 6107–6112.
[21] D. A. Shultz, M. G. Hollomon, *Chem. Mater.* **2000**, *12*, 580–586.
[22] G. Bringmann, T. Pabst, S. Busemann, *Tetrahedron* **1998**, *54*, 1425–14385.
[23] H. M. Kim, C. Jung, B. R. Kim, S.-Y. Jung, J. H. Hong, Y.-G. Ko, K. J. Lee, B. R. Cho, *Angew. Chem.* **2007**, *119*, 3530–3533; *Angew. Chem. Int. Ed.* **2007**, *46*, 3460–3463.
[24] S. A. Martin-Brown, Y. Fu, G. Saroja, M. M. Collinson, D. A. Higgins, *Anal. Chem.* **2005**, *77*, 486–494.
[25] V. H. J. Frade, M. S. T. Gonçalves, P. J. G. Coutinho, J. C. V. P. Moura, *J. Photochem. Photobiol. A* **2007**, *185*, 220–230.
[26] a) D. M. Adams, L. Noodleman, D. N. Hendrickson, *Inorg. Chem.* **1997**, *36*, 3966–3984; b) D. M. Adams, D. N. Hendrickson, *J. Am. Chem. Soc.* **1996**, *118*, 11515–11528.
[27] N. Vân Anh, R. M. Williams, *Photochem. Photobiol. Sci.* **2012**, *11*, 957–961.
[28] a) J. Crank, *The Mathematics of Diffusion*, Clarendon Press, Oxford, **1975**; b) J. Siepmann, F. Siepmann, *Int. J. Pharm.* **2011**, *418*, 42–53.
[29] a) H. B. Hopfenberg in *Controlled Release Polymeric Formulations, Vol. 33* (Eds.: D. R. Paul, F. W. Harris), ACS symposium Series 33, American Chemical Society, Washington, **1976**, pp. 26–32.
[30] Z. Ramtoola, O. I. Corrigan, C. J. Barrett, *J. Microencapsulation* **1992**, *9*, 415–423.
[31] V. Knorr, L. Allmendinger, G. F. Walker, F. F. Paintner, E. Wagner, *Bioconjugate Chem.* **2007**, *18*, 1218–1225.
[32] R. Sens, K. H. Drexhage, *J. Lumin.* **1981**, *24*, 709–712.

Received: July 9, 2013
Published online: November 20, 2013

